NASA Technical Memorandum 83015
AIAA-82-1938

Rail Accelerator Research at Lewis Research Center

W. R. Kerslake and B. Z. Cybyk
Lewis Research Center
Cleveland, Ohio

Prepared for the
Sixteenth International Electric Propulsion Conference
cosponsored by the American Institute of Aeronautics and Astronautics,
the Japan Society for Aeronautical and Space Sciences,
and Deutsche Gesselschaft fur Luft- und Raumfahrt
New Orleans, Louisiana, November 17-19, 1982

NASA

RAIL ACCELERATOR RESEARCH AT LEWIS RESEARCH CENTER

by W. R. Kerslake and B. Z. Cybyk

National Aeronautics and Space Administration
Lewis Research Center
Cleveland, Ohio 44135

ABSTRACT

A rail accelerator has been chosen for study as an electromagnetic space propulsion device because of its simplicity and existing technology base. This paper presents both the results of a mission feasibility study using a large rail accelerator for direct launch of ton-size payloads from the earth's surface to space, and the results of initial tests with a small, laboratory rail accelerator. The laboratory rail accelerator has a bore of 3 by 3 mm and has accelerated 60 mg projectiles to velocities of 11 to 864 m/s. Rail materials of Cu, W, and Mo have been tested for efficiency and erosion rate.

INTRODUCTION

An electromagnetic space propulsion program at Lewis Research Center (LeRC) consists of two main parts - studies and feasibility research. Studies are performed to establish merit and define potential space applications that would benefit through the use of electromagnetic propulsion. Research is performed to mitigate technical uncertainties and establish feasibility of the concept. One of the concepts under investigations is an electromagnetic rail accelerator.

Electromagnetic launcher concepts go back to early 1900's, but materials design concepts, and inability to rapidly switch high current at high voltage, limited achievable projectile velocities to hundreds of meters/second. Improvements in the 1940-1960 period increased achievable velocities to a few km/s, and a technical breakthrough in 1972 (ref. 1) enabled a velocity of 6.2 km/s to be reached using a rail accelerator. This breakthrough used an insulated projectile and a plasma armature to drive the projectile and overcame a fundamental limit of projectile melting due to the need of passing the accelerating current through the projectile itself.

A rail accelerator mission that recently has been studied is the direct launch of radioactive waste payloads from the earth's surface to deep space and the launch of cargo and consumables to earth orbit. A solar system escape mission requires a minimum launch velocity of 16.7 km/s. With atmospheric drag and other losses included, the actual launch velocity may be near 20 km/s for solar system escape and 5 to 10 km/s for earth orbital missions. Such velocities are believed by rail accelerator researchers to be achievable and are the goal of present research programs.

Reference 2 presents a detailed study which defines a feasible "reference concept" rail accelerator system and a cost estimation to build and operate the system to launch ton-size payloads directly from the earth's surface. The first part of this paper summarizes the results of this study and presents drawings of the concept. Reference 3 developed an earlier idea of using a small bore rail accelerator to eject a continuous stream (5 Hz) of pellets as a reaction engine for orbit raising missions. Reference 3 shows that a reaction engine rail accelerator system performance could be

competitive with an ion thruster system, but that two major problems existed. These problems are that the rail accelerator would have to eject ten million pellets to perform a typical mission, and a large part of these pellets would go into near earth orbits and be a potential hazard for future spacecraft.

The last part of this paper presents the experimental results of a 3-mm square bore rail accelerator tested at Lewis Research Center during 1981 and the first half of 1982. Other researchers (refs. 4 to 7) have been testing rail accelerators more extensively with larger bores. The objectives of other researchers include impacting pellets at high speeds (5 to 25 km/s) to study the equation-of-state for solid materials and a variety of military applications.

SYMBOL LIST

E_p	projectile energy, J
E_R	energy to rails, J
ESRL	earth to space rail launcher
F	Lorentz force, N
g	gravity, 9.806 m/s^2
G-10	fiberglass laminate
I_R	rail current, A
ℓ	length of pendulum target, mm
L	inductance, H
L'	inductance gradient of rails, H/m
M_p	mass of projectile, gm
M_T	mass of pendulum, gm
P_R	power to rails, W
t	time projectile in accelerator, s
V_B	breech voltage, V
V_C	capacitor bank voltage, V
v_f	final velocity of projectile, m/s
x	projectile acceleration distance, mm
θ	half angle of pendulum swing, deg

EARTH TO SPACE LAUNCHER CONCEPT

Battelle Columbus Laboratories was contracted by LeRC to perform an assessment of a concept to use a rail accelerator to launch ton-size projectiles from the earth to space. The full results of this assessment including system capital and operating costs are given in reference 2, Projectile Designs.

Two missions were studied, mission A, the launch of nuclear waste material to solar system escape, and mission B, the launch of nonfragile payloads to earth orbit. The table below lists the size and mass of the projectiles designed for each mission.

SIZE OF PROJECTILES AND LAUNCH TUBE

Parameter	Mission A	Mission B
Payload, kg	250	650
On board propulsion, kg	0	1575
Total launch mass, kg	2055	6500
Projectile diameter, m	0.51	0.91
Launcher bore, m (square)	0.67	1.00
Launch acceleration, g's	10 000	2500
Launcher length, m	2000	2000
Launch angle from horizon	90	20

Figures 1(a) and (b) are drawings of the projectile design. For mission A the payload, 250 kg of nuclear waste, is surrounded by a 12-cm thick steel shield. A sabot fits around the projectile at two places to electrically insulate the projectile and to fit the round projectile to the square bore of the rail accelerator. The sabot is designed of interlocking pieces that separate away from the projectile as it leaves the accelerator tube. A tapered nose cone provides a low drag configuration for atmospheric flight and fins provide stability. The projectile is launched vertically at dawn from the earth's equator so that a minimum velocity is required for solar system escape (16.7 km/s with no air drag). Once launched correctly, no further trajectory corrections are needed. Incorrect launches are handled via a "fault tree" presented in reference 2.

The projectile design for mission B is some what similar to mission A, but larger. It is also cylindrical in shape with an aerodynamic nose cone and fins. A heavy shield is not needed, but a chemical rocket system is required for orbit insertion. Again a sabot is used to insulate and seal the bore. Launch velocities are approximately 5 km/sec to raise the payload to near-earth orbit.

Launcher Designs

Figure 2 shows sketches of the two launcher systems. The launcher for each mission is a 2 km-long underground shaft lined with two parallel copper rails. Each set of copper rails is divided into 10 000 segments. Electric current, fed into each segment, passes through a plasma behind the projectile and produces a Lorentz force which accelerates the payload along the rails. The Lorentz force (j x B) applied to rail geometry is: $F = 1/2 L' I^2$, where L' is the rail inductance per meter and I is rail current. The launcher is vertical for mission A (solar system escape) to minimize escape velocity and atmospheric drag. The launcher for mission B is 20° up from the horizon. The 20° angle is a trade-off between atmospheric drag and the most desirable launch angle (90°) for near earth missions.

Energy for launching is obtained from a nuclear power plant located near the launch site. See figure 3 for a drawing of the launch site and various support facilities. The energy for each rail segment is stored in a 60 MJ homopolar generator. The homopolar generator is used as an intermediate store before transferring its energy into a large aluminum inductor. As the projectile plasma passes the start of each segment, the inductor stored energy flows through the plasma and across to the other rail. Details of the homopolar generator installation are shown in figure 4. A new rail segment begins every 20-cm. As the homopolar generators are about 1.5 m diameter, they are designed in a spiral fashion as shown in the side view. The

cross section, top view, shows the arrangement of LN_2-cooled aluminum inductors and the supporting structure for the entire assembly.

Cost Analysis

Reference 2 estimates the total research, development, and capital costs for the facility to do both missions A and B at a cost of 5 to 8 billion dollars (1981). If two launches per day are made for mission A, the total United States waste from commercial power plants in the year 2020 could be safely disposed in deep space. The costs (including a 30-yr amortization of total investment) of disposing nuclear waste with the rail launcher would be $550/kg. For the sake of comparison, today's launch cost using the shuttle would be 30 to 50 times greater. The cost of transporting bulk cargo payload to earth orbit would be $590/kg or about 5 to 8 times less expensive than using the present shuttle. Eight mission B launches per day (5200 kg) payload would provide for resupply of manned space station consumables for estimated needs in the year 2020.

Concept Study Conclusions

The study of reference 2 concluded that a large rail accelerator launcher was technically feasible and environmentally and economically viable. Basic technology advances are needed to store and switch the large quantities of electrical energies (600 GJ at 28 MA) used in the launcher. Also no one has ever constructed a rail accelerator of the size required (1 m bore by 2000 m long). Present technology rail accelerators have centimeter-size bores and are a few meters long. They use a level of 0.5 to 1.5 MJ and 1 MA of current. Scaling studies with rails of a 1/2-centimeter to 5-centimeter bore (ref. 8) show no surprises nor arc instabilities. Given modest funding support, the authors believe 40 years to be a reasonable time to develop rail accelerator technology to the point required for the large launchers described above.

Small Rail Accelerator Tests

To gain a first hand understanding of the physics of electromagnetic rail accelerators, a small 5 kilojoule (kJ) rail accelerator was designed and tested at LeRC. Even though this 5 kJ accelerator is too short and too small for high performance tests, some interesting trends were noted. A series of systematic tests of various rail materials, projectile starting position and bore clearances, and energy levels were made by several student engineers and a visiting university staff member. Recognition is given to: Sharon Rutledge and Marco Brdar for constructing the apparatus and performing initial tests, to Alan Reilly for running later tests (beyond this paper's deadline, June 1982); and to Bohdan Cybyk for the operation and analysis of most of the results presented below.

APPARATUS

The size and construction details of the rail accelerator, used in tests reported here in (unless otherwise noted) are shown in figure 5. The metal rails were clamped with thick sheets of a fiberglass laminate (G-10) and six screws. The height of the rails was 3 mm and the length was 50 mm. A 3 by 3 by 6 mm-long polycarbonate (lexan) projectile was fit between the rails.

The spacing between rails was maintained during assembly by inserting a square mandrel into the bore while tightening the six screws. The mandrel cross section was equal to the projectile cross section. The screw holes permitted enough clearance for about 0.25-mm bore width variation. Once the mandrel is removed, friction maintained the rail position. Maximum rail movement was limited by the clearance of the clamping screw holes. A small, U-shaped piece of aluminum foil (6 by 2 by 0.025 mm) was wrapped around the back of the projectile and was pinched between the projectile and rails. The back of the projectile was located 13 mm into the breech of the accelerator as shown in figure 5. Rail materials tested were copper, tungsten, molybdenum, and aluminum.

The experimental tests were grouped into three parts, loose-fitting projectiles, tight-fitting projectiles, and miscellaneous tests. For the loose fitting tests, the projectiles were hand-cut and generally about 0.3 mm smaller than the rail height. The tight-fitting projectiles were 0.05- to 0.08-mm smaller than the bore size. Several miscellaneous tests; plugged breech, thin rails, cross shaped projectiles, and reverse rail current were conducted and will be described in the RESULTS AND DISCUSSION section.

The capacitor energy storage bank and electrical schematic are shown in figure 6. Unless otherwise noted, the capacitor bank consisted of 16 capacitors with an average of 108 μF capacitance each, connected in parallel and rated for 2 kV maximum voltage. They were charged with a 10-mA power supply which was disconnected before discharging the bank. Discharge current was carried by copper straps. A mechanical vacuum switch was used as a closing switch. Breech voltage, (using high voltage probe) and current (using either a Rowgoski or Pearson coil) were recorded on an oscilloscope.

The projectile final velocity was measured using a pendulum target shown in figure 7. The target surface of the pendulum consisted of 10-mm deep putty layer that captured the projectile with no rebounding. The swing of the pendulum was recorded by electrically sparking a trace on paper from a rod on the pendulum to a ground plate beneath the paper. The typical traces recorded were 5- to 15-cm long. The velocity of projectile was calculated using:

$$v_f = \frac{M_l + M_p}{M_p} \sqrt{2g(1 - \cos \theta)\ell}$$

where θ is the half angle swing of the pendulum.

The accuracy of measuring the width of pendulum swing was 0.5 mm. This accuracy results in a v_f uncertainty of 8 m/s. The length of the pendulum was measured directly to be 1232-mm and compared against a length calculated from swing period measurement, $l = g \times (\text{period}/2\pi)^2$, of 1226 mm. The length calculated from swing period was assumed to give the more correct pendulum characteristic and was used to calculate the velocities presented herein. The distance from the rail accelerator muzzle to the pendulum target was 300 mm. The loss of v_f due to atmospheric air drag was calculated to be 2.3 percent of v_f using a drag coefficient of one. If this loss of velocity were to be included, the values of v_f in tables I to III would be 2.3 percent greater. Figure 8 is a photo of part of the bank, copper circuit, rail accelerator, and pendulum target.

PROCEDURE

The metal rails, lexan projectile and fuse were weighed before each test. The rails and projectile were weighed afterwards. If the rails had been previously used, they were sanded smooth and cleaned in dilute HCl to remove any residue before the next test. The rails, projectile and fuse were assembled and bolted to the load terminals of the circuit. The bank was charged to the desired voltage in the range of 500 to 2000 volts and then discharged into the rail assembly. The bank was allowed to ring until the energy discipated. After a rail accelerator test, approximately 20 to 50 volts remained in the bank.

The ringing of the bank and circuit with a copper bar short across the load terminals is shown in figure 9. The bank was charged to 1000 volts. The ringing period of 260 μs and decay envelope gave a circuit induction of 0.97 μH and a circuit resistance of 4.4 mΩ. Figure 10, 11, and 12 give current and breech voltage traces for typical firings at 2000, 1500, and 1000 volts respectively. Also plotted are the accelerator input power which is the product of current and breech voltage and the arc resistance which is arc voltage divided by rail current. The time at which the projectile left the accelerator was taken to be $t = 2x/v_f$; where x is 37-mm, the projectile accelerating length, and v_f is the projectile final velocity measured by the pendulum target. As seen in figure 10, the projectile left the accelerator in shorter time with higher bank voltage. The ringing frequency and shape of current and breech voltage traces were relatively unchanged by the rail system, projectile mass, or with value of bank voltage. The inductance and resistance of the rails is small compared to the external circuit. As expected, the rail current and voltage decreased with bank voltage decrease.

The energy expended in the rail accelerator test was calculated by integrating the power-time curve:

$$E_R = \int_0^t P_R(t)dt$$

where t is the exit time of the projectile.

An effective inductance gradient, L', was calculated for each test by the following equation:

$$L' = \frac{2M_p v_f}{\int_0^t I_R^2(t)dt}$$

where I_R is the rail current.

RESULTS AND DISCUSSION

The results of 56 test firings of a 3- by 3-mm bore rail accelerator are presented. The tests are divided into three groups; loose-fit projectiles, tight-fit projectiles, and miscellaneous tests. The specific data for each firing are listed in tables I, II, and III, respectively. The test numbers are in chronological order and are the actual experiment log test numbers.

Where tests or data are not included in the tables, the tests were redundant, bad or the data not obtained. The loose fit projectile tests were made early in the program when a number of varables were being scanned. Later, in an attempt to increase accelerator efficiency, tight-fit projectiles were made with closer bore tolerance.

All of the tests in the first two groups use the same rail accelerator geometry as shown in figure 5. The last group of miscellaneous tests was done with a varity of geometries for specific test reasons, and each will be discussed.

Loose-Fit Projectile Tests

The objectives of these tests were: (1) to measure final projectile velocity reproducibility of the rail accelerator; (2) to measure final projectile velocity as a function of rail current and rail material; and (3) to measure rail erosion as a function of rail current and rail material.

The reproducibility of final projectile velocity for the same bank voltage was in fair agreement as can be seen in table I, i.e., tests 22, 30, and 32. For some tests the final velocity repeated within ± 5 percent, while other tests, the final velocity spread was ± 12 percent. Reasons for these velocity spreads could be the following: (1) inconsistant loss in the circuit closing switch, which used 40 percent of the test energy; (2) variation in capacitance of bank (some intermittant open cans were found and subsequently replaced); or (3) inaccuracies in pendulum target measurements.

Figure 13 shows the energy efficiency of the projectile (projectile energy divided by input rail energy) plotted against maximum rail current. The efficiency is low because of the relatively low final velocities with such a short accelerator. The energy lost in the arc is very large compared to the energy gain at low projectile velocities. As can be seen in figure 13, the projectile efficiency rises quickly with I_R because the arc losses tend to be fixed with time and a greater fraction of the energy goes into the projectile. Projectile efficiency is calculated on the basis of the integrated power going into the accelerator rather than on bank energy because nearly 60 percent of the bank energy is lost in the closing switch (40 percent) and external bank circuit (20 percent).

A truer measure of the rail accelerator performance may be seen in the L' value. The value of L' can be thought of as a measure of the net force accelerating the projectile and can be compared to an ideal (where all flux lines react with the normal current to accelerate the projectile) Lorentz force based on rail geometry and I_R. As can be seen in figure 14, values of L' show no increase nor decrease with I_R for the loose fit tests, and are low compared to values of 0.5 to 0.6 $\mu H/m$ usually quoted for good rail accelerator performance. Reasons for low L' values are: (1) much of the arc blows backward and burns outside the breech, hence the I_R^2 force does not act on the projectile; (2) wide rails with low geometric inductance gradient; (3) any of the classic rail accelerator loss mechanisms, such as, plasma blow by, rail friction, or projectile-rail pinching. The vertical spread of the data of figure 14 could be the result of any combination of the above reasons.

Rail erosion as seen from table I increased with bank voltage. The rail material type showed the following order of least to greatest erosion: tungsten, molybdeunum, and copper. The erosion pattern on the rails was

similar from test to test. The length and amount of rail damage was two-thirds behind the projectile starting position (about 10 mm) and one-third downstream. The surface roughness pattern on the rails was almost equal to the rail height at the projectile starting position and then tapered to no roughness as the projectile moved downstream. Microscopic examination of the rail surface indicated: (1) micro balls of solidified molten metal; (2) ridges of jagged metal pulled up from the surface; and (3) deposits of copper oxide when copper rails were used. The edges of the rails seemed to have a smoother surface and the greatest net loss of material. Figure 15 is an open-lens photograph of a test firing in a darkened room. Streaks of light are assumed to be molten bits of the copper rails. Rebounding of these bits can be noticed in the picture. Notice that most of the arc luminosity is out the breech end with little muzzle flash. The bank was charged to 750 volts for this test, but data were not included in this report because a different closing switch was used for this test. (This closing switch was subsequently replaced because it was believe to bounce after closing.)

Evidence of condensed copper vapor and copper oxide was seen on the mating surfaces of the rails and G-10 clamped insulators. The maximum lateral depth of penetration of this vapor between the rails and G-10 insulator was about 10-mm and occurred at the projectile starting position. The depth of penetration and thickness of deposits became less for positions both upstream (backwards) and downstream. The penetration of these vapors may be evidence that the screws holding the accelerator together were too small and physical separation of the rails and G-10 occurred. The lexan projectile mass lost during a test was low. Mass losses were 0.001 gram or less for all tests listed in tables I, II, and III.

Perhaps the most interesting results of these loose-fit projectile tests were that: (1) rail projectiles could be accelerated at 300 000 g's even though the rail-projectile gap area was 10 percent of the projectile area and an open breech was used; and (2) a ringing pulse discharge circuit could operate a rail accelerator. As seen in figures 10 to 12, the arc goes out and must restrike every time the arc voltage goes through zero. This process results in an average arc resistance that is higher than would be for a steady arc. Note that the arc resistance is not minimum at maximum arc power, but that it occurs about 20 to 50 μs later. A time varying arc may offer diagnostic advantages to study the dynamic characteristics of a rail accelerator arc.

Tight-Fit Projectile Tests

The objectives of these tests were to improve the projectile final velocity by closing the gap between rail and projectile, and to obtain additional erosion data for various types of rail materials. The tight-fit projectile tests are listed in table II. The projectile masses for the tight-fit tests were about 10-percent greater than for the loose fit tests because the projectiles were made larger to more closely fit the bore.

The first result noted was a higher projectile velocity for the same bank voltage, in spite of the larger projectile mass. This result can be seen by comparing similar voltage tests between tables II and I. The velocities with tight-fit projectiles average 10- to 20-percent higher than for loose-fit projectiles. Tight-fit projectiles resulted in even higher increases in projectile efficiency and L'. These increases may be seen in figures 13 and 14, where projectile energy efficiency is almost doubled for

the tight-fit projectiles. Figure 14 shows an L' gain of almost 50 percent for the tight-fit projectiles. The obvious conclusion is that a tight-fit projectile has less plasma blow by and is more effectively accelerated. Note that one tight-fit test, number 76, had a considerably lower L' than the others. The reason for this result might be pinching of rails ahead of the projectile, or expansion of the G-10 sides permitting blow-by.

Another reason, however, for the greater acceleration of the tight fit projectiles may be the larger rail erosion for these tests comparing copper rail tests 65B, 68, and 71 (tight fit) with tests 48, 51, and 53 (loose fit), it is seen that the tight fit tests resulted in twice as much rail erosion. Perhaps this erosion mass added to, and increased, the accelerating gas-plasma pressure.

A trend can be seen between projectile velocity and copper rail erosion by comparing tests 65B, 68, 71, and 74 of table II. These tests are plotted in figure 16 for easy comparison of this trend, which was to have the largest velocity produced for the first test of a set of rails. Each subsequent test resulted in lower projectile velocity and lower rail erosion. The authors believe that with each test of a set of rails, the rail-projectile fit deteriorated, permitting more plasma blow-by, less plasma density, and less rail erosion at the lower plasma density. Finally, after four tests (with Cu rails) the deterioration equaled the gap of a loose-fit test and so did the rail accelerator performance. (The subscripts on the rail material symbol represent the number of times tested for that rail set). Also plotted on figure 16 is the rail erosion for other types of rail material. As can be seen, there is no trend between number of tests and rail mass lost, but the projectile velocity is usually lower as more tests are made.

The pattern of rail erosion with the tight-fit tests was similar to that described for the loose-fit tests, that is, about two-thirds of the erosion occurred behind the projectile starting position. The erosion pattern downstream of the starting position gradually tapered towards the center of the rail and then disappeared. The rails were sanded between firings to remove surface roughness and give a reasonably close fit. An interesting observation was noted after multiple firings, namely, that the volume lost from the rails was occurring at the top and bottom of the rail, rather than the center of the rail where the visible surface roughness occured. Some of the missing volume undoubtedly occurred during the hand sanding of the rails between the tests, but the authors feel that the hand sanding was carefully done and could not account for the bulk of missing rail material. We therefore postulate that some rail erosion mechanism may be removing rail material from the edge of the rail and depositing it at the centers, or that the erosion rate is greater at the rail edges.

The same order of rail erosion with material type was found as for the loose-fit tests, namely, the greatest rail mass lost was for aluminum and copper rails with the refractory metals molybdenum and tungsten being considerably lower in erosion. For rail erosion measured on a volume basis, aluminum rails with a low density showed the greatest volume lost. Tests with aluminum rails were accompanied by an extremely bright flash, probably aluminum vapor burning in air. After a test the aluminum rail surface showed severe erosion and loss of material along the entire length. The purpose of trying aluminum rails was to see if the great number of aluminum atoms lost from the rails would improve the projectile acceleration, even more than the velocity improvement during the copper rail tests (65B, 68) with high rail erosion. The result with the aluminum rails, however, was not to increase the projectile acceleration as much as was contemplated.

Tests 98 and 97, table II, were an attempt to achieve higher projectile velocity by using a larger capacitor bank (adding more capacitors in parallel). The result was indeed a larger projectile velocity by almost 30 percent for a 50 percent increase in bank energy at the same bank voltage. The L' for these tests 98 and 97, however, were 30- and 20-percent lower than the regular capacitor bank tests for Cu and W rails respectively. Also, the rail erosion was about 50 percent higher when using the larger bank. The conclusion was that the larger bank produced larger projectile velocities, but at a cost of lower performance (lower L') and higher rail erosion. The lower L' may have been caused by the higher repulsive forces on the rails allowing increased plasma blow-by. (The values of I_R max for most of table II were unavailable due to a late triggering scope. In most tests, however, the second I_R (negative) peak was obtained and used with a known current reversal ratio to estimate I_R max. These estimated I_R max values are isted in table II and are believed to be accurate to $\pm$10 percent.)

Miscellaneous Tests

A number of miscellaneous tests were conducted to gain an insight into a number of parameter changes. The results of these tests are summarized in table III and are described below.

Cross-shaped projectile. - The purpose of this test was to intentionally increase the blow-by of a projectile to study the resulting loss of performance. The projectile used in tests 29 of table III was made of a lexan block, 3 by 3 by 6 mm long and similar to the projectiles of table I but with a 1 mm square cut out of each corner for the full length of the projectile. This cut 44 percent out of the projectile cross sectional area. As can be seen in table III, test 29, this projectile resulted in a larger velocity than for corresponding tests, table I, tests 23, 31, or 34. However, a comparison of L' values for the same tests show that the cross-shaped projectile had an L' about 10 percent lower than the average. This small reduction of L' indicates that projectile blow-by may not be as serious a problem as formerly believed, and more tests should be made to quantify the plasma blow by losses. For example, the cross-shape projectile could be expected to have lower friction retarding force, but the relative magnitude of friction forces are difficult to determine.

Hi L rails. - One reason for the low L' values of tables I and II is that the width of the metal rails (see fig. 5) gave a low electrical inductance. Tests 43, 44, and 45 were an attempt to improve the rail electrical inductance by "removing metal" from the rails. This was done as shown in figure 17. Instead of the normal rail design, the rails were cut down to a square cross section and the void volume filled with a slab of G-10 material. The result of using the Hi L rails was a 40-percent increase in projectile velocity and a 30-percent increase in L'. This result can be seen by comparing tests 43, 44, and 45 (table III) with Tests 22, 30, and 32 (table I). The increased performance was nice, but still nowhere near an L' of 0.5 or 0.6 μH/m that is typical of good performance.

The probable reason for the lower than desired L' for tests 43, 44, and 45, was probably the same reason that all the open breech tests were low L', namely a major portion of the arc current blew out the breech and established an arc in the air behind the rails. This air arc was no where near the projectile and thus could not accelerate it down the rails. Because of the small rail accelerator geometry, no attempt was made to measure the relative magnitude of the actual current inside the accelerator.

Another possible reason for low L' on tests 43, 44, and 45 lies in rail distortion during the firing. For each test, the rails partly separated from the epoxy bond to the G-10. This ocurred at either the breech or muzzle end, curving inward, leaving a permanent set in the rail. It is not known if this inward rail movement occurred before or after the projectile traveled past that part of the rail. If before, the rail possibly pinched the projectile.

Breech-plugged tests. - Tests 49 and 86 represent two tests where the breech was plugged. In test 49, the breech was filled with putty for inertial confinement. In test 86 a second projectile was glued in the breech. In both tests, the same projectile starting position was used (37 mm from muzzle end) and a void space of about 1 mm existed between the plug and back face of the projectile.

Test 49 was performed using the Hi L rail geometry (fig. 17). The putty plug was blown out during the firing, but as seen in the test 49 data (table III) compared to earlier Hi L tests, the projectile velocity was double and the effective L' value more than doubled. This performance increased was undoubtedly due to increase acceleration by the trapped gases. Perhaps the electric arc was also trapped and the I_R^2 accelerating force was also greater. The rail erosion for test 49 was about double that for the open breech tests (test 43 and 44).

Test 86 was performed using a standard rail geometry (fig. 5). In this test the breech plug remained in place during the firing. The projectile velocity was tripled compared to similar (Tests 40, 47, or 50, table I) tests with an open breech. The effective L' value for test 86 was a remarkable 0.78 μH/m. This L' value exceeds the maximum geometrical L' value of 0.6 (for square bore with square rails) and is a clear example of acceleration aided by gas expansion. The rail erosion data was not reported due to difficulty in removing the breech plug after the test.

Tests 49 and 86 show that most of a rail accelerator projectile's initial acceleration can be due to gas force rather than electrical force. Depending on the experimenter's goals and the robustness of his accelerator design, he may choose to take advantage of this early gas force or not. Based on these two tests with a very small rail accelerator, the gas force cannot be used to prevent major rail erosion in the breech area, and the design of a rail accelerator for many firings should try a different technique to avoid rail erosion. (Note, many rail accelerator researchers believe that an initial projectile velocity of 0.3 to 1.0 km/s will reduce rail erosion, permitting hundreds of firings before major rail refurbishment).

Reverse rail current test. - Test 60B of table I represents one of several tests conducted to differentiate between gas force and electrical force. The rails for test 60B were configured as sketched in figure 18. A standard 50 mm-long accelerator (fig. 5) was used, but the projectile was positioned 13 mm from the nominal muzzle end together with a standard aluminum foil fuse (also at 13 mm from muzzle). Then the entire accelerator was turned around and connected as shown in figure 18. The rail current now passes into the "new muzzle" end and produces no I_R^2 accelerating force on

the projectile. The full I_R current, however, passes through the aluminum fuse and can cause a gas accelerating force. The resulting projectile velocity, from gas acceleration was only 29 m/s or about 7-percent of the energy normally imparted to the projectile for a comparable test (test 22, 30, or 32 table I). The authors believe this test only indicates a minimum ratio between initial gas and electric force for an open breech design, but suggests that for most of the open breech tests reported herein, electric forces were primarily responsible for the observed acceleration.

Half-length projectile tests. - Tests 89, 92, and 90 were performed using the standard (fig. 5) accelerator with a tight-fit projectile, only the projectile was now a 3 mm cube (half the nominal projectile length). Nearly twice the projectile velocity was obtained using these half-mass projectiles (compared to tests 67, 70 and 73, or test 658 and 68, all in table II). The L' values for the half-length projectiles were somewhat (5 to 10 percent) higher than for the same compariable tests noted above. This suggests that the quicker acceleration for the half-length projectiles resulted in a shorter time for the arc to blow back into the air, and perhaps increased the fraction of current remaining inside the rails. Thus, there was more electrical force and higher L'.

6 by 6 mm bore test. - One test was performed using a 6 by 6 mm bore by 100 mm long rail accelerator. The results of testing this accelerator are listed as test 94, table III. The projectile velocity was very low, 35 m/s, but this was due to the limited energy in the capacitor bank and the relatively large projectile mass. (6 by 6 by 12 mm size, lexan). The L' value, 0.15 μH/m per meter was surprisingly high and compared favorably with similar loose fit projectile tests (tests 48, 51, or 53, table I). Tests of 6 by 6 mm bore accelerators were not continued because of the mismatch between accelerator size and available bank energy.

Long rail tests - Several tests were conducted with a 3 by 3 mm bore by 90 mm long rail accelerator. Except for the length, the accelerator was constructed as shown in figure 5 (10 screws were used for assembly instead of 6). Tight-fit lexan projectiles were used. The results of two of the tests with the 90 mm-long accelerator are listed as tests 106 and 107 in table III. Higher projectile velocities were achieved with the longer accelerator than for comparible tests at the same bank energy with the 50 mm standard length (Tests 65B or 91, table II). The higher velocities were due to: (1) a longer acceleration time in the bore, and (2) a 19 percent lighter mass projectile. The L' values for the long accelerator tests were about 20 percent lower. This suggests that the velocity losses due to rail friction may have been greater than velocity gained due to either the tail end energy of the I_R ringing pulse, or the somewhat lighter projectile that was used.

Mid-start projectile position. - Several tests (Tests 103-105 table III) were made to see if reduced projectile friction would result in significantly greater projectile velocity. The projectile was started mid way down the accelerator, that is, the back face and aluminum fuse were 25 mm from both the muzzle and breech ends. The velocities achieved with these mid-start tests were remarkably high for the short distance in the bore, even higher than for tests at the same bank energy and a normal starting position (Tests 65B, 68, or 71). In retrospect, the high velocities achieved could have resulted from three factors: (1) less friction loss due to the shorter

acceleration path, (2) more gas force due to more gas restriction (longer bore length) on the breech end; or (3) less arc blow back to outside with more arc current remaining inside for I_R^2 acceleration. Further tests are required to identify or separate the relative magnitude of each of the above factors.

CONCLUDING REMARKS

This paper has presented two topics: one, a design study to launch ton-size projectiles from earth to space using a very large rail accelerator; the other, results of testing a very small laboratory rail accelerator at Lewis Research Center.

The design study has shown the feasibility of using a large rail launcher to dispose of nuclear waste material in deep (solar system escape) space, or to send bulk cargo to earth orbit. Such a launcher facility would cost less than $8 billion (1981 dollars), would launch space payloads at a cost 5 to 50 times less than using the present space shuttle, and would have a 30 year pay back time. Although study has shown the launcher concept to be potentially feasible, many technology advances are required to manage the large electrical energies needed, and a probable time to readiness is 40 years.

The results of 56 test firings of a small (3 by 3 mm) bore rail accelerators using a 5 kJ capacitor bank were presented. Erosion rates for various materials and current densities were obtained. Tungsten rails had the least erosion, but copper rails may be acceptable if initial acceleration is given to the projectile before entering the rail accelerator. Insights were gained on projectile plasma blow-by, arc blow-back, and breech plugging.

An additional study to define missions that can be benefically achieved with electromagnetic mass accelerators has begun. Also a more energetic capacitor bank (240 kJ) has been obtained for testing larger bore (6 by 6 mm and 12 by 12 mm) laboratory rail accelerators.

REFERENCES

1. Barber, J. P., "The Acceleration of Macroparticles and a Hypervelocity Electromagnetic Accelerator," The Australian National Univeristy, EP-T12, 1972.
2. Rice, E. E., Miller, L. A., and Earhart, R. W., "Preliminary Feasibility Assessment for Earth-to-Space Electromagnetic (Rail gun) Launchers," NASA CR-167886, June 1982.
3. Bauer, D. P., and Barber, J. P., "The Electric Rail Gun for Space Propulsion," NASA CR-165312, Feb. 1981.
4. Hawke, R. S., Brooks, A. L., Fowler, C. M., and Peterson, D. R., "Electromagnetic Rail Gun Luanchers: Direct Launch Feasibility," AIAA Journal, Vol. 20, No. 7, July 1982, pp. 978-985.
5. Fowler, C. M., Peterson, D. R., Caird, R. S., Erickson, D. J., Freeman, B. L., and King, J. C., "Explosive Flux Compression Generators as Rail Gun Power Sources," Los Alamos Nation Laboratory, Report LA-UR-80-2542, 1980; also the IEEE Transactions on Magnetics, Vol. 18, Jan. 1982, pp. 64-67.
6. Deis, D. W., and McNab, I. R., "A Laboratory Demonstration Electromagnetic Launcher," IEEE Transactions on Magnetics, Vol. 18, No. 1, pp. 16-22, Jan. 1982.

7. Shrader, J. E., and Bjorkman, M. D., "Design and Performance of a Capacitor Powered Rail Gun," Paper 5A5, IEEE International Conference on Plasma Science, Ottawa, Canada, May 1982.
8. Brooks, A. L., Hawke, R. S., Scudder, J. K., and Wozynski, C. D., "Design and Fabrication of Large and Small Bore Rail Guns," Lawrence Livermore Laboratory, UCRL-84876, Nov. 1980.

TABLE I. - LOOSE FIT PROJECTILE-RAIL ACCELERATOR TESTS (Bank Cap., 1740 μF)

Test number	Rail material	V_C, V	v_f, m/s	t, μs	Projectile acceleration, m/s^2	M_p, mg	E_p, J	E_R, J	Projectile efficiency, percent	$I_R$max, ka	L' μH/m	Rail loss, mg
36	Cu_3	500	11	6470	0.018×10^5	67	0.004	113	0.004	16	0.06	(2)
22	Cu_6	1000	111	667	1.7	68	.42	----	------	34	.15	----
30	Cu_1	↓	119	624	1.9	56	.40	----	------	---	-----	13
32	Cu_2	↓	113	657	1.7	67	.43	467	.09	36	.15	----
56	Cu_9	↓	97	760	1.3	63[a]	.29	487	.06	↓	.12	4
58	Cu_{11}	↓	47	1570	.3	123[a,b]	.14	486	.03	↓	.11	0
23	Mo_8	↓	88	820	1.1	68	.27	409	.07	↓	.12	---
31	Mo_1	↓	111	666	1.7	68	.42	----	------	↓	.15	0
24	Mo_2	↓	87	856	1.0	58	.22	433	.05	↓	.10	2
25	W_8	↓	95	785	1.2	67	.30	438	.07	↓	.12	---
33	W_1	↓	101	735	1.4	72	.37	416	.09	↓	.14	0
35	W_2	↓	92	804	1.2	61	.26	438	.06	35	.11	1
48	Cu_5	1500	262	283	9.2	59	2.1	747	.27	54	.12	27
51	Cu_6	↓	305	243	12.5	58	2.7	645	.42	52	.14	17
53	Cu_7	↓	226	329	6.9	59	1.5	----	----	---	-----	21
46	Mo_3	↓	237	313	7.6	62	1.8	----	----	---	-----	4
52	Mo_4	↓	262	283	9.2	59	2.0	670	.30	54	.12	0
54	Mo_5	↓	247	300	8.2	57	1.8	678	.26	52	.11	2
41	W_3	↓	262	283	9.3	60	2.1	747	.28	53	.12	1
47	W_4	↓	278	267	10.4	63	2.4	739	.33	57	.14	0
50	W_5	↓	270	274	9.8	56	2.1	742	.27	55	.12	5
61	W_6	2000	446	166	26.8	59	5.9	1206	.49	75	.12	24
62	W_7	2000	492	151	32.6	60	7.3	1178	.62	77	.14	14

Note: Subscript number on rail material is number of times that rail was fixed.
[a]18 mg Al wire fuse used instead of standard, 0.8 mg Al foil fuse.
[b]Projectile made of teflon instead of lexan.

TABLE II. - TIGHT FIT PROJECTILE-RAIL ACCELERATOR TESTS (Bank Cap., 1740 μF)

Test number	Rail material	V_C, V	v_f, m/s	t, μs	Projectile acceleration, m/s^2	M_p, mg	E_p, J	E_R, J	Projectile efficiency, percent	$I_R$max, ka	L' μH/m	Rail loss, mg
65B	Cu_1	1500	357	199	18.6×10^5	75	4.77	590[c]	0.81	(55)[b]	0.23	46
68	Cu_2	↓	335	221	15.1	75	4.20	640[c]	.66	↓	.20	45
71	Cu_3	↓	295	252	11.7	75	3.21	685[c]	.47	↓	.18	33
74	Cu_4	↓	258	288	8.9	74	2.46	720[c]	.34	↓	.15	19
67	W_1	↓	323	230	14.0	75	3.91	710[c]	.55	↓	.19	13
70	W_2	↓	347	214	16.2	75	4.51	700[c]	.64	↓	.21	12
73	W_3	↓	327	226	14.4	75	4.00	710[c]	.56	↓	.20	13
76	W_4	↓	250	296	8.4	75	2.35	760[c]	.31	↓	.15	3
66	Mo_1	↓	311	238	13.0	73	3.51	670[c]	.52	↓	.18	12
69	Mo_2	↓	303	245	12.3	76	3.43	680[c]	.51	↓	.18	16
72	Mo_3	↓	263	283	9.2	74	2.54	710[c]	.36	↓	.15	14
75	Mo_4	↓	307	241	12.7	74	3.48	670[c]	.52	↓	.18	11
77	Al_1	↓	311	239	13.0	75	3.62	----	----	↓	.19	32
91	W_2	2000	502	148	34.0	77	9.68	794	1.22	74	.21	16
95	W_4	2000	496	149	33.2	75	9.35	800	1.17	75	.20	20
98	Cu_3	1500[a]	405	183	22.0	73	5.96	----	----	(64)[a]	(.14)	65
97	W_1	1500[a]	450	165	27.2	74	7.47	----	----	(64)[a]	(.16)	20

[a]Bank capacitance increased to 2620 μF; ringing period of arc, 320 μs; (I_R)max, 64 KA (est).
[b]No record of (I_R)max available, I_R wave form taken from table I tests.
[c]Average arc energy of table I used.

TABLE III. – MISCELLANEOUS TESTS WITH RAIL ACCELERATOR (BANK CAP., 1740 μF)

Test number	Test geometry	Rail material	V_c, v	V_f, m/s	t, μs	Project acceleration, m/s^2	Mp, mg	E_p, J	E_R, J	Project efficiency, percent	$I_R$max, ka	L', μH/m	Rail loss, mg
29	Cross projectile,	Mo_{10}	1000	119	622	1.9×10^5	42	0.30	376	0.08	34	0.11	---
43	Hi L rails	Cu_1	1000	154	480	3.2	59	.70	---	---	---	---	5
44	Hi L rails	Cu_1	↓	154	480	3.2	69	.81	434	.19	36	.19	7
45	Hi L rails	Cu_1	↓	162	455	3.5	58	.76	431	.18	36	.17	---
49	Hi L rails, Breech plug	Cu_1	↓	308	240	12.8	59	2.79	484	.58	33	.40	12
86	Breech plug, firmly placed	W_6	1500[d]	864	86	101.0	75[a]	28.00	557	5.03	55	.78	---
60B	Reverse rail current	Cu_{15}	1000	29	2550	.1	63	.03	486	---	30	---	---
89	Half-length projectile	W_1	1500[d]	622	119	52.0	37[a]	7.14	424	1.68	57	.21	6
92	Half-length projectile	W_3	↓	566	131	43.0	39[a]	6.25	490	1.28	56	.22	7
90	Half-length projectile	Cu_4	↓	589	126	47.0	37[a]	6.42	424	1.51	(54)[b]	.23	29
94	6 by 6 mm bore	Cu_2	↓	35	2110	.1	600	.37	---	---	(57)[b]	.15	16
106	Long rails, 90 mm	Cu_1	↓	457	272	13.6	61[a]	6.35	820	.77	56	.19	43
107	Long rails, 90 mm	Cu_1	2000[d]	635	196	26.2	61[a]	12.29	1257	.98	77	.16	82
103	Mid start[c]	Cu_1	1500[d]	363	138	26.4	76	4.95	505	.98	(53)[b]	.32	78
104	Mid start[c]	Cu_2	1500[d]	392	128	30.7	78	5.89	498	1.18	(53)[b]	.35	47
105	Mid start[c]	Cu_3	1500[d]	380	131	28.9	77	5.40	480	1.12	(50)[b]	.38	47

[a]Tight-fit projectiles.
[b](I_R)max based on average of other tests at similar conditions.
[c]Normal 50 mm long accelerator used; projectile back face start position, 25 mm from muzzle.
[d]Bank capacitance, 1780 μF.

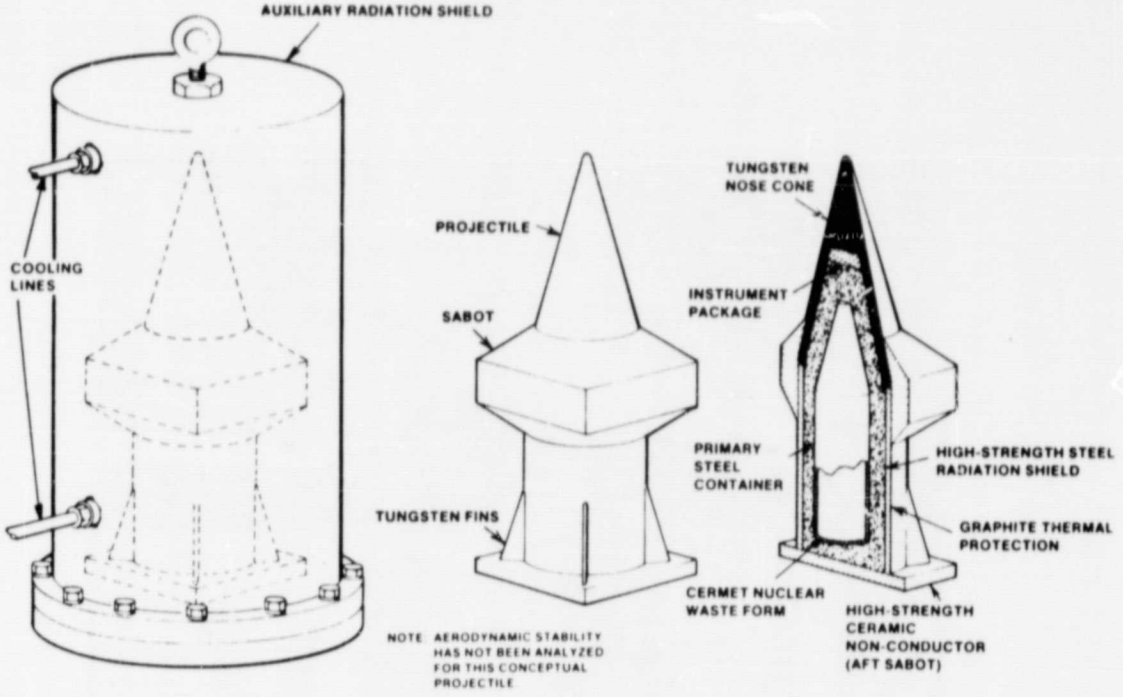

(a) ESRL projectile concept for nuclear waste disposal in space.

Figure 1. - Projectile design.

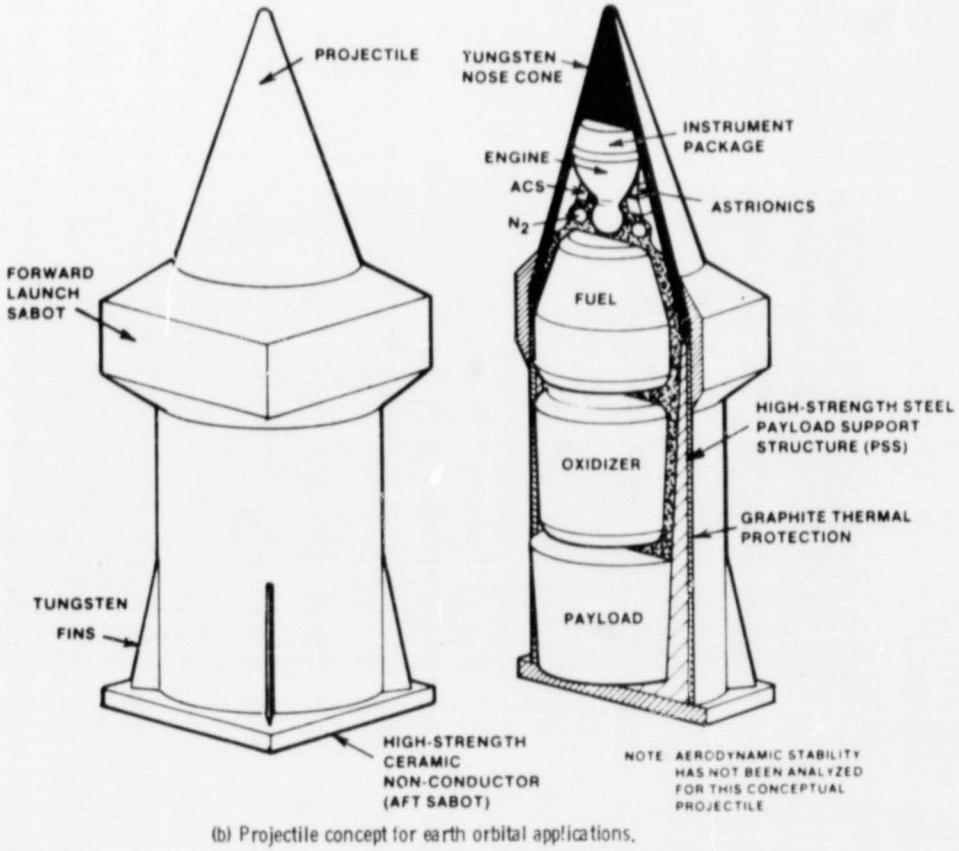

(b) Projectile concept for earth orbital applications.

Figure 1. - Concluded.

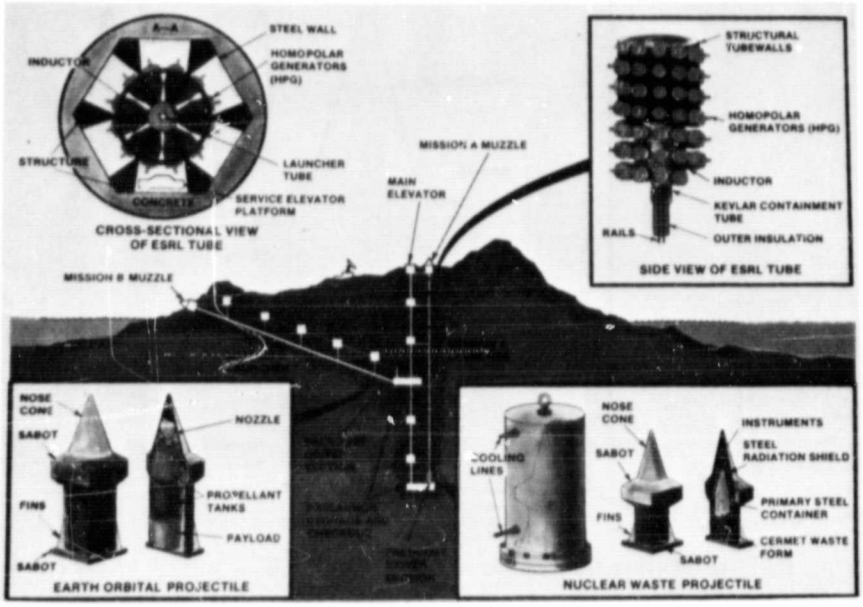

Figure 2. - Side view of rail launcher facility, each launcher tube is 2km long.

C-82-3135

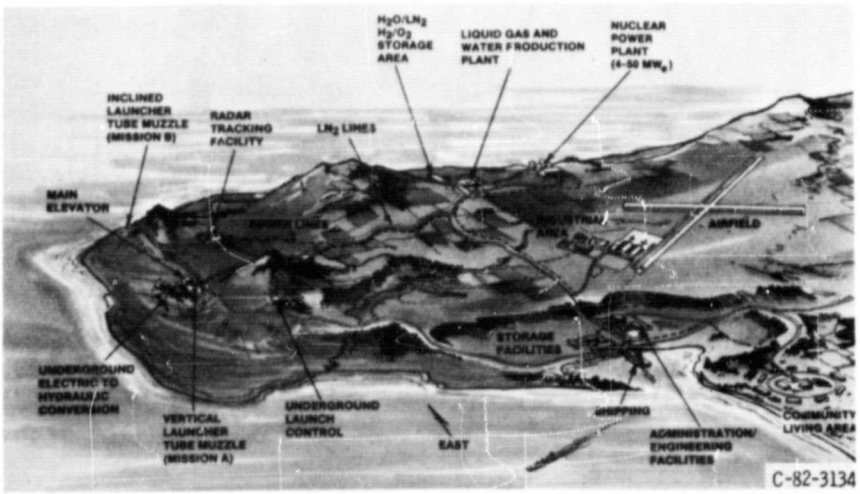

Figure 3. - Drawing of rail launcher support facilities.

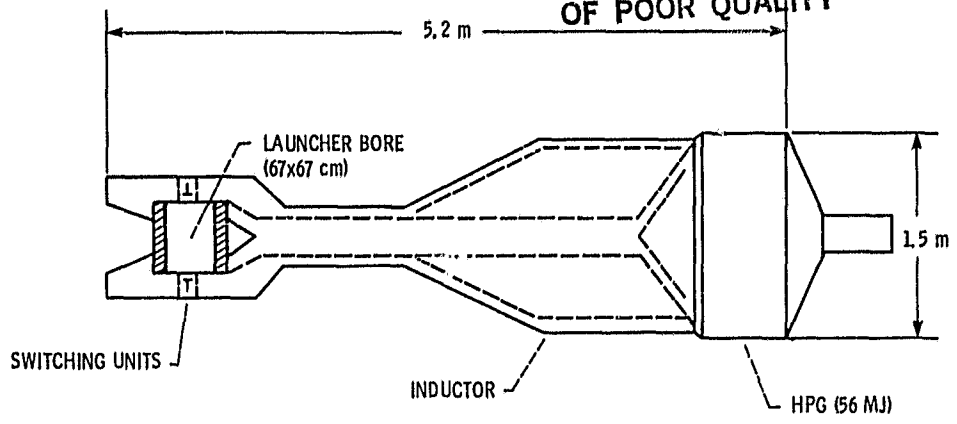

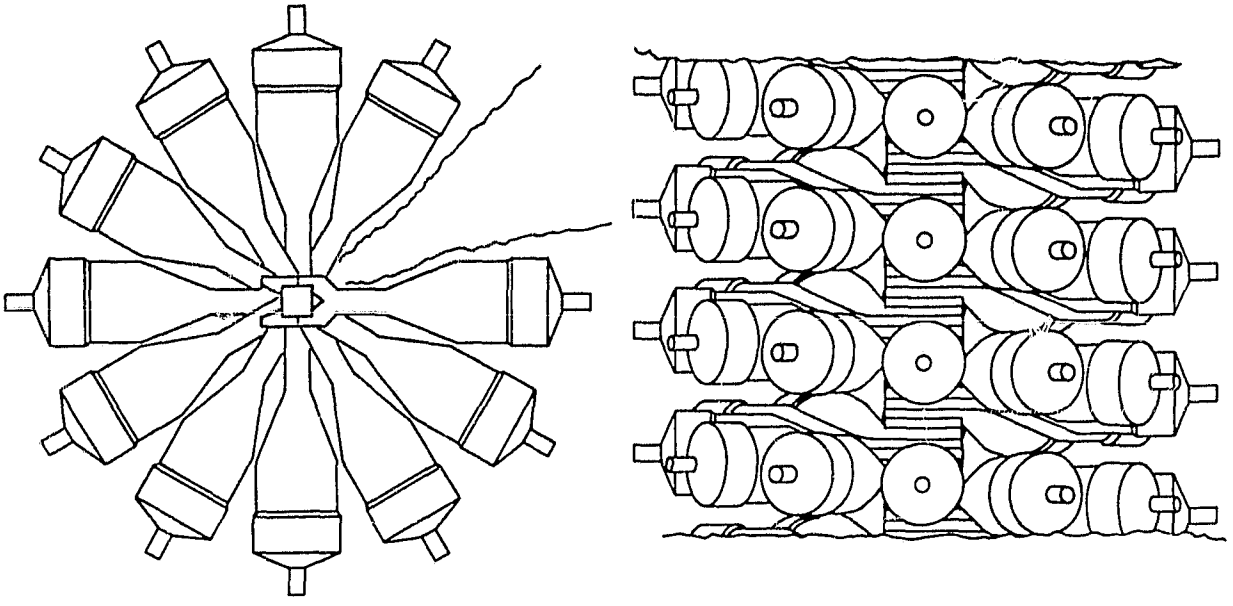

(a) Single homopolar generator (HPG)- inductor energy store unit.
(b) Assembled system of HPG's.

Figure 4. - Spiral arrangement of energy stores around center line of launcher tube.

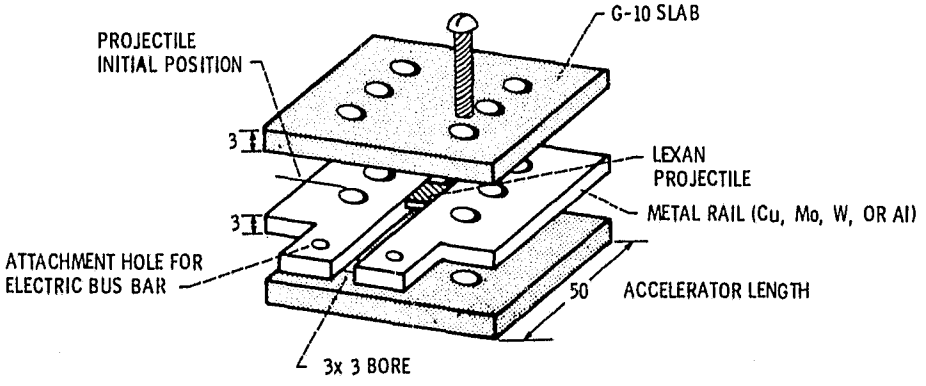

Figure 5. - Sketch of small rail accelerator construction details (all dimensions in mm).

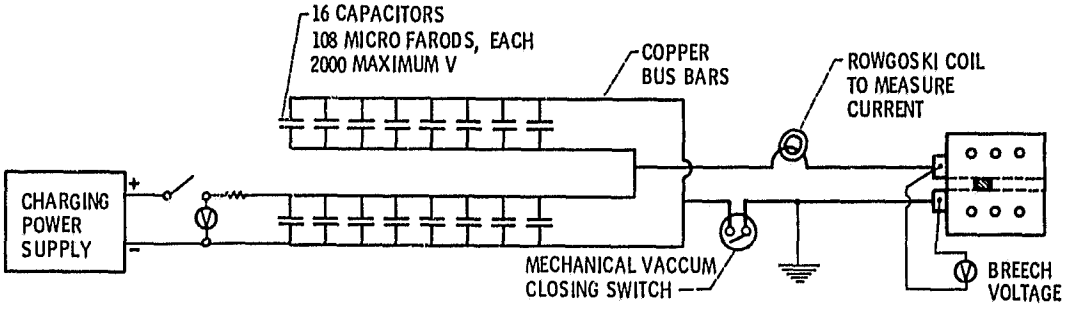

Figure 6. - Electrical schematic of capacitor bank used to fire small rail accelerator.

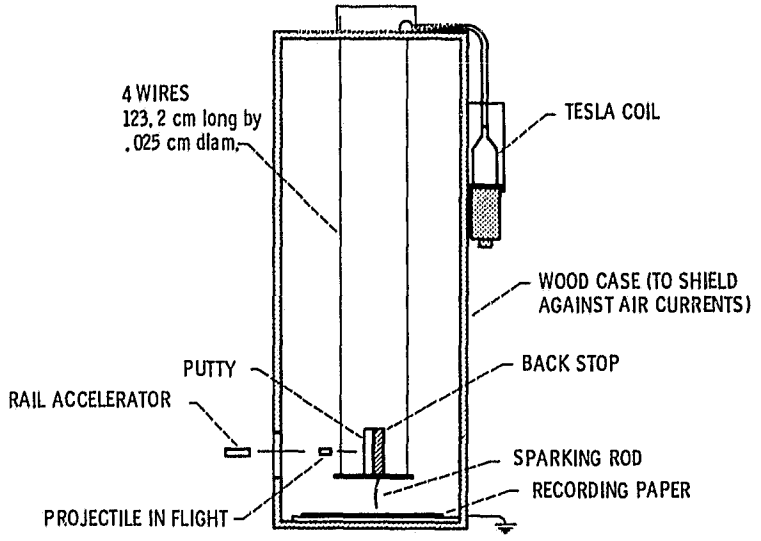

Figure 7. - Details of pendulum target used to measure projectile velocity. (Total mass of pendulum, 214 gm.)

Figure 8. - Photograph of capacitor bank, rail accelerator, and pendulum target.

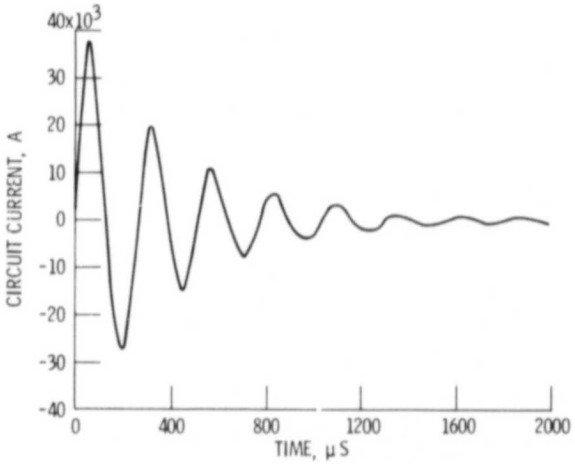

Figure 9. - Short across load terminals. Bank voltage, 1000 V Bank capacitance, 1740 μf (16 CANS).

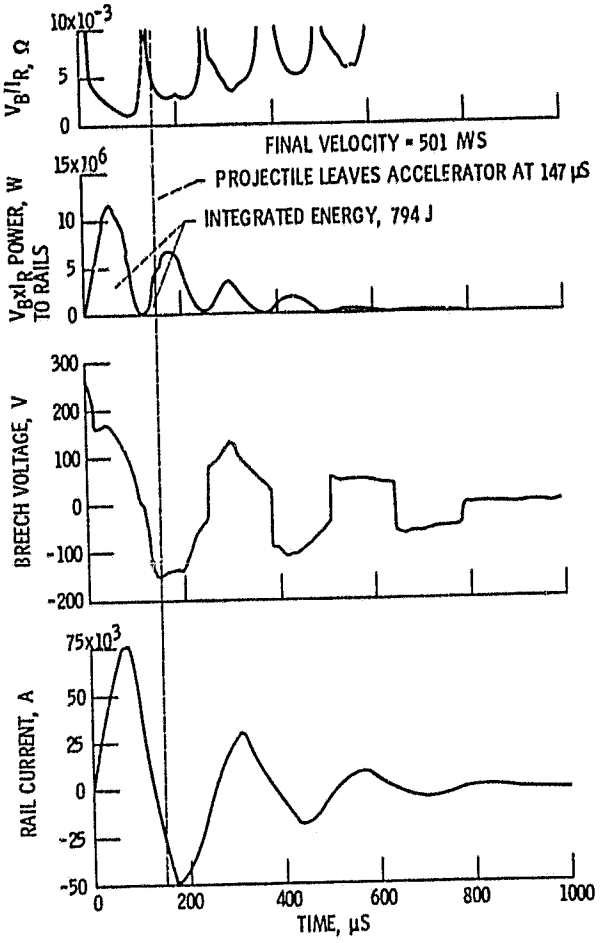

Figure 10. - Data traces for test at 2000 V bank voltage. (Tungsten rails, test91, tight fit projectile).

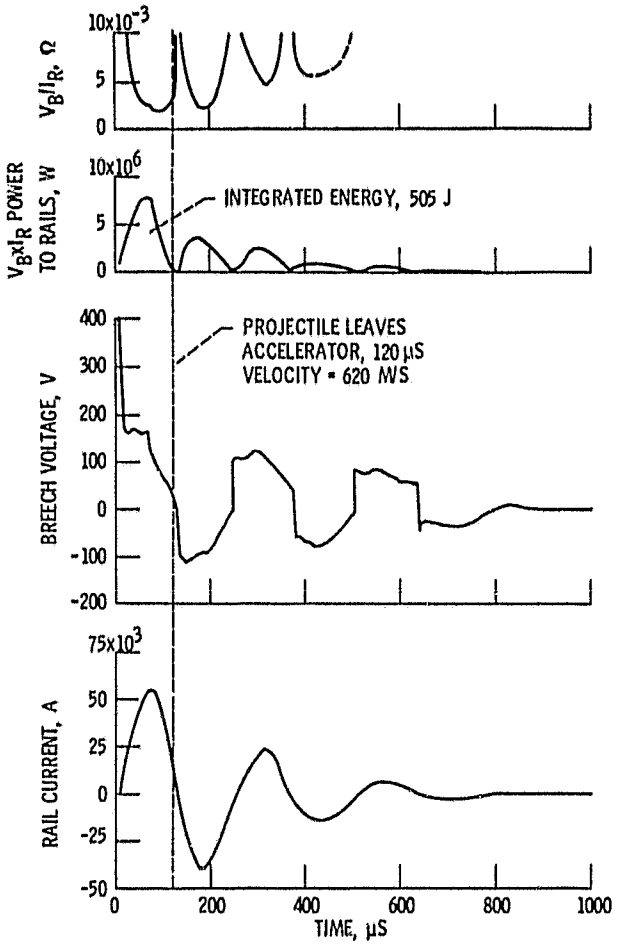

Figure 11. - Data traces for test at 1500 V bank voltage. (Tungsten rails test 89, tight fit projectile, 1/2 mass).

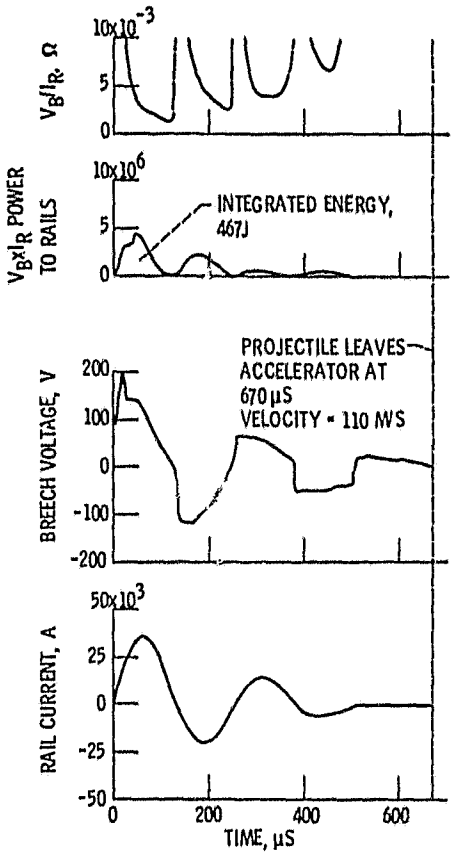

Figure 12. - Data traces for test at 1000 V bank voltage. (Copper rails, test 22, loose fit projectile.)

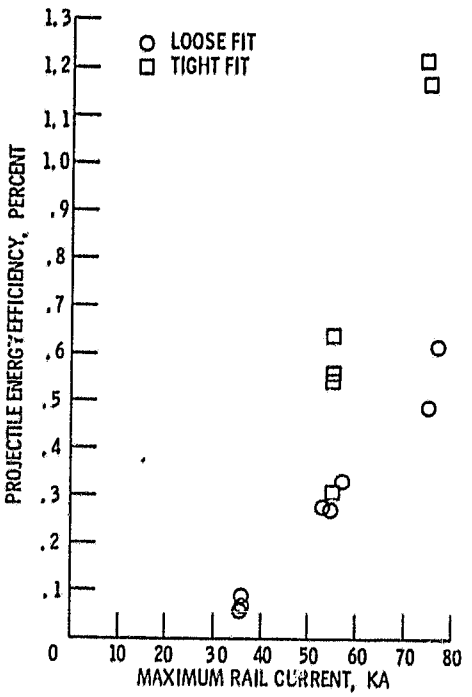

Figure 13. - Projectile efficiency as function of rail current. Tungstn rails.

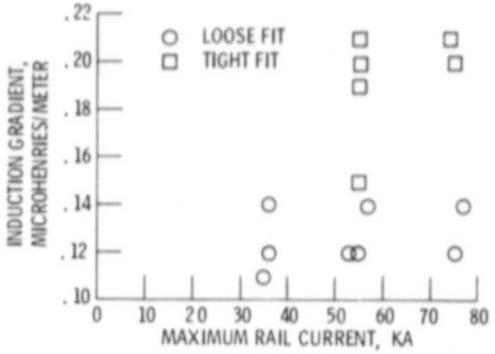

Figure 14. - Rail accelerator inductance gradient as function of rail current. Tungsten rails.

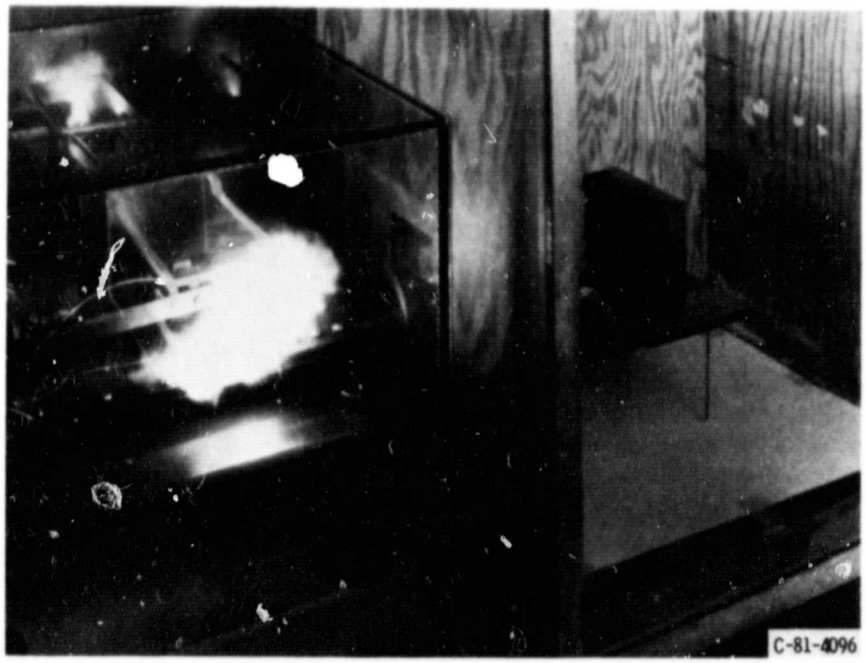

Figure 15. - Open lens of rail accelerator test firing. Bank voltage, 750 v. (early model closing-switch seen in reflection of left corner of photograph.)

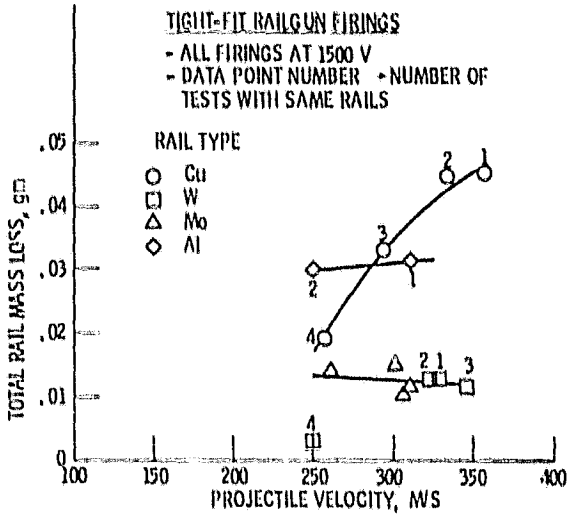

Figure 16. - Projectile final velocity as a function of rail erosion and number of reused tests. (Data point subscript is number of times that rail was used.)

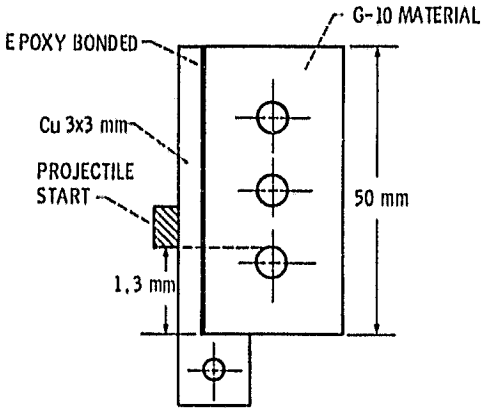

Figure 17. - Thin rail accelerator design (left rail not shown).

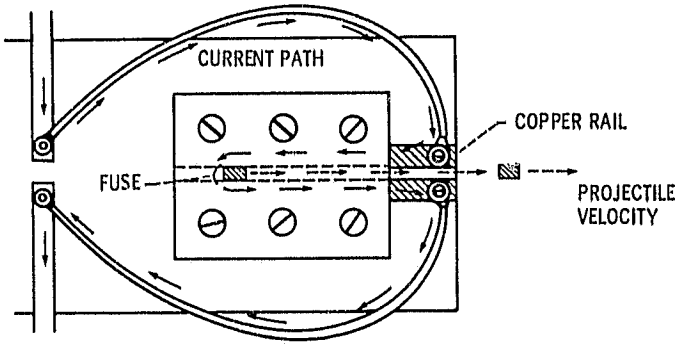

Figure 18. - Reverse current test of rail accelerator.